

Enhanced Dielectric and Energy Storage Properties of the (200)-oriented Plate-like $\text{Na}_{0.5}\text{Bi}_{0.5}\text{TiO}_3$ /Polyimide Composite Materials

Shuangshuang Yue¹, Baoquan Wan¹, Haiyu Li¹, Yunying Liu², Qiwei Zhang^{1,*}

¹ School of Materials and Metallurgy, Inner Mongolia University of Science and Technology, 7# Arding Street, Kun District, Baotou 014010, China

² School of Chemistry and Chemical Engineering, Inner Mongolia University of Science and Technology, 7# Arding Street, Kun District, Baotou 014010, China

*E-mail: zqw8000@imust.edu.cn

Received: 27 September 2018 / Accepted: 5 November 2018 / Published: 5 January 2019

Ferroelectric/polymer composites capable of possessing high dielectric constant, excellent flexibility and withstanding high electric field have been considered as promising candidates for embedded capacitor applications, or other energy storage/transfer devices. However, conventional ferroelectric particle composites only exhibit high dielectric enhancement at a high fraction, and cannot withstand high breakdown electric fields. Compared with particle fillers, the plate-like ferroelectrics with obvious anisotropic dielectric behaviors exhibit excellent dielectric properties in a co-plane orientation. Here we reported a new polyimide based composite material with the (200) oriented plate-like $\text{Na}_{0.5}\text{Bi}_{0.5}\text{TiO}_3$ powders as fillers. The results showed that the plate-like $\text{Na}_{0.5}\text{Bi}_{0.5}\text{TiO}_3$ fillers lead to a obviously increase of dielectric constant for polyimide composites ($\epsilon_r=14.00$) at a very low content when $\text{Na}_{0.5}\text{Bi}_{0.5}\text{TiO}_3$ content is about 5 wt%, which is 4.03 times as large as that of pure polyimide ($\epsilon_r=3.47$) while maintaining a relatively low loss ($\text{tg}\delta=0.0061$) and high breakdown strength (1412 kV/cm). The measured energy density with 5 wt% $\text{Na}_{0.5}\text{Bi}_{0.5}\text{TiO}_3$ content increased to a value of 1.24 J/cm³, higher than that of pure polyimide (0.67 J/cm³). The result indicates that the composite could have potential applications in embedded capacitors and microelectronic applications.

Keywords: Polymer-matrix composites; Plate-like ferroelectrics; Dielectric constant; Energy density; Embedded capacitors

1. INTRODUCTION

Dielectric materials have been attracting more and more attention with the ever-growing market of demands from mobile electronic devices, hybrid electric vehicles, medical implants, and other

technologies [1,2]. They have big advantages of fast charging-discharging and high power density, compared with other energy conversion and storage system, such as batteries, fuel cells, and electrochemical capacitors [3,4]. Nowadays, driving by the device development towards miniaturization, lightweight and integration, dielectric materials with high power density, high energy density, excellent flexibility, fast charging-discharging process and broad operating temperature range are required [5-8]. However, their applications are limited by low energy density. In principle, the energy density (U_e) can be determined by electric field (E) and dielectric constant (ϵ_r) for linear dielectric materials:

$$U_e = 1/2 \epsilon_r \epsilon_0 E^2 \quad (1)$$

for non-linear dielectric materials, the energy density (U_e) is given by:

$$U_e = \int_0^{Max} \epsilon_0 \epsilon_r E dE \quad (2)$$

where ϵ_r is relative dielectric constant, ϵ_0 is the dielectric constant of free space ($= 8.85 \times 10^{-12} \text{ Fm}^{-1}$), and E is the applied electric field. From the above formula, it is found that the energy density is related extremely with the dielectric constant and breakdown strength. Thus, it is necessary to investigate a desired dielectric material with high dielectric constant and electric breakdown strength, fabricating high energy-storage capacitors [9-11].

In order to achieve excellent flexibility and high energy density, ferroelectrics with high dielectric constant are generally introduced into polymer matrix by controlling microstructures of fillers or interfacial modifications between two phases [12,13]. Especially, different morphologies of ferroelectrics play a very important role in improving overall dielectric properties for ferroelectric/polymer composites, such as ferroelectric particles (0D or 3D) or fibers (1D) with different shapes [14]. However, for particulate polymer composites, a required high concentration of ceramic particles usually results in an obvious decrease in flexibility and breakdown strength. Meanwhile, many pores, voids or other structural imperfections are also involved in composites. Fibers as fillers with a large aspect ratio are capable of improving the dielectric constant of the composites at much lower volume fractions due to their large dipole moments, which have been widely investigated [15-17].

In contrast, the plate-like ferroelectrics with a desired orientation and high aspect ratio possess strong anisotropic dielectric behaviors, whose dielectric constant in a co-plane orientation is obviously higher than that of other planes [18]. But, plate-like ferroelectrics are usually considered as template particles, which are added into piezoelectric materials to form textured ceramics by the templated grain growth (TGG) method, finally to obtain high-performance piezoelectric materials [19]. If ferroelectric materials with 2D plate-like structure would be introduced into polymers, it is possible to achieve excellent dielectric properties and dielectric breakdown strength due to superior anisotropic dielectric feature and 2D plate-like structure, as well as 1D fiber fillers has a large aspect ratio [20-23]. Although the dielectric constant is dramatically increased compared with the polymer matrix, there still exists space to improve overall dielectric properties.

Recently, Wang et al. fabricated plate-like $(\text{Ba}_{0.6}\text{Sr}_{0.4})\text{TiO}_3$ /poly(vinylidene fluoride) (PVDF) textured composites using a tape casting and hot pressing method. The dielectric constant and dielectric loss are 62.2 and 0.042 up to a loading of 40 vol %, respectively. The average dielectric breakdown strength is up to 151.9 kV/mm [24]. Luo et al. fabricated plate-like BaTiO_3 /rGO/P(VDF-HFP) three-phase composites, the dielectric loss of graphene/P(VDF-HFP) composites can be well suppressed. A

high dielectric constant of 66.2 and the suppressed dielectric loss of 0.048 are simultaneously obtained [25].

Among many polymers, polyimides (PI) are considered to be one of the most important high performance materials due to their high tensile strength superior mechanical properties, high glass transition temperature, good resistance to solvents and excellent thermal stability [26-28]. Thus, PI is suitable for application in dielectric storage devices as a high temperature resistant polymer matrix. Many efforts have been afforded to achieve excellent dielectric properties by introducing different kinds of ferroelectric or metal oxide materials [29-35]. For example, Liu et al. reported that GPTS-SiO₂@GO/PI nanocomposite films by in-situ polymerization. The GPTS-SiO₂@GO/PI composite had an increased dielectric constant of 79 and a decreased loss of 0.25 at 40 Hz as the fraction of GPTS-SiO₂@GO was 20 wt% [36]. Beier et al. fabricated homogenous Ba_{0.7}Sr_{0.3}TiO₃ (BST) nanocrystal/PI composite, whose dielectric constant is only 6.2 at 1 MHz, and an enhancement of 24% in breakdown strength is obtained at 10 vol % BST [37]. Sun et al. fabricated BaTiO₃/PI composite with enhanced dielectric permittivity (6.8) and low dielectric loss (0.012) [38]. Choi et al. fabricated INAAT-BaTiO₃/PI and APTS-BaTiO₃/PI composite. The polyimide composite with BaTiO₃ particles (BaTiO₃ content at 50 vol.%) treated by INAAT showed an increased dielectric constant of 19.03 while retaining an appropriate dielectric loss of 0.0109, as compared to the dielectric constant (14.64) of polyimide/APTS-treated BaTiO₃ composite [39]. However, the mechanical properties and the processability of PI-(based) composites would be dramatically reduced when ceramic filler fraction is up to 20 vol% [40]. The energy storage properties of ferroelectric/polyimide nanocomposites were listed in Table 1. How to obtain high dielectric constant and high energy density in ferroelectric/PI composites is still a big challenge.

Up to now, only a few works on plate-like ferroelectric/polymer composites are reported. Therefore, it is important to systematically investigate the effects of plate-like ferroelectrics on dielectric constant and energy storage density for other polymer-based composites, especially for PI-based composites. In this paper, the plate-like Na_{0.5}Bi_{0.5}TiO₃ (BNT), fabricated by two-step molten salt method, is introduced to polyimide (PI) matrix. The microstructure and energy storage properties are systematically investigated. The dielectric constant and energy storage density of composite materials can be significantly improved due to anisotropic dielectric behaviors of plate-like BNT.

2. EXPERIMENTS

2.1. Materials

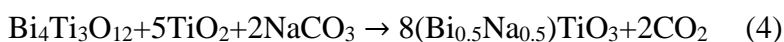
Bi₂O₃ (99.9%), TiO₂ (99.8%), NaCO₃ and NaCl (99.8%) were purchased from Alfa Aesar(China) Chemicals Co., Ltd. 4,4'-Diaminodiphenyl ether (ODA), pyromellitic anhydride (PMDA) and N, N-dimethylformamide (DMF, SP grade) were purchased from Aladdin, Shanghai, China. Hydrogen peroxide (H₂O₂, 30 wt%) and (3-Aminopropyl)triethoxysilane (KH550) were purchased from Beijing Reagent Co. Absolute alcohol (AR grade) was purchased from Tianjin Reagents Co. Ltd. All the reagents were used as received without further purification. Deionized water was applied by our laboratory.

2.2. Plate-like BNT fabrication

The (200)-oriented plate-like BNT powders were fabricated by a conventional two-step molten salt method. Firstly, Bi₂O₃ and TiO₂ as starting raw materials were weighted for synthesizing plate-like Bi₄Ti₃O₁₂ powders according to the equation:



The weighted powders in a mixed molten salt [NaCl: (Bi₂O₃+TiO₂)=1:1(weight ratio)] were calcined at 1100 °C for 2h. Subsequently, the calcined powders were washed with de-ionized water (100 °C) for several times until no Cl ions could be detected. Secondly, the as-prepared Bi₄Ti₃O₁₂ powders, Na₂CO₃ and TiO₂ were homogeneously mixed according to the following equation:



These powders in equation (4), excessive Na₂CO₃ (20 wt%) and NaCl molten salt in a weight ratio (1:1) were carefully milled with alcohol and zirconia grinding media in polypropylene bottles for 24 h. After drying, the mixture was placed in a sealed alumina crucible and heated at 900 °C for 2h. After the obtained powders were washed with HNO₃ and de-ionized water for several times, the plate-like BNT powders were successfully obtained.

2.3. Functionalization of the plate-like BNT

The prepared BNT platelets were functionalized by KH550 referred to previous reports [41-44]. Specifically, BNT platelets was firstly dispersed in 200 mL H₂O₂ (30 wt%) using an ultrasonic processor to increase the hydroxyl groups, the mixture was sonicated for 30 min and refluxed at 106 °C for 5 h. The hydroxylated BNT was dispersed in an appropriate amount of KH550 hydrochloride aqueous solution at 80 °C for 10 h. The powders were separated by centrifugation and rinsed repeatedly with excess deionized water or absolute ethanol. In this process, the -Si-O- bond and amide bond were generated by the react of KH550 with hydroxylated BNT powders and PAA respectively. The detailed experimental procedure is listed in Figure 1 (a) and (b). This shows that the KH550 played a bridge role between BNT platelet and PAA, which not only facilitates the homogeneous dispersion of BNT fillers in polymer matrices, but also passivates the surface of BNT fillers.

2.4. Preparation of BNT/PI composite materials

The BNT/PI composites films were fabricated by in situ polymerization. The composite films were prepared by blending as follows. First, the ODA was dispersed into the DMF solvent, and stirred until the ODA was completely dissolved in the DMF solvent. Then the BNT powders were added into the solution with an ultrasonicator of 1h until to form the suspensions with the contents of 0wt%, 1wt%, 3wt%, 5wt%, and 7wt%, and stirred for 5 h. Subsequently, PMDA was added slowly to make sure the complete dissolution, and then stirred for 24 h after ultrasound for 30 minutes. Finally, this suspension was cast onto clean glass and dried for 40 min at 80 °C under vacuum, and then dried at 150°C/1h, 200°C/1h, 250°C/1h and 300°C/1h to convert completely into BNT/PI composites films. The detailed experimental procedure is listed in Figure 1 (c).

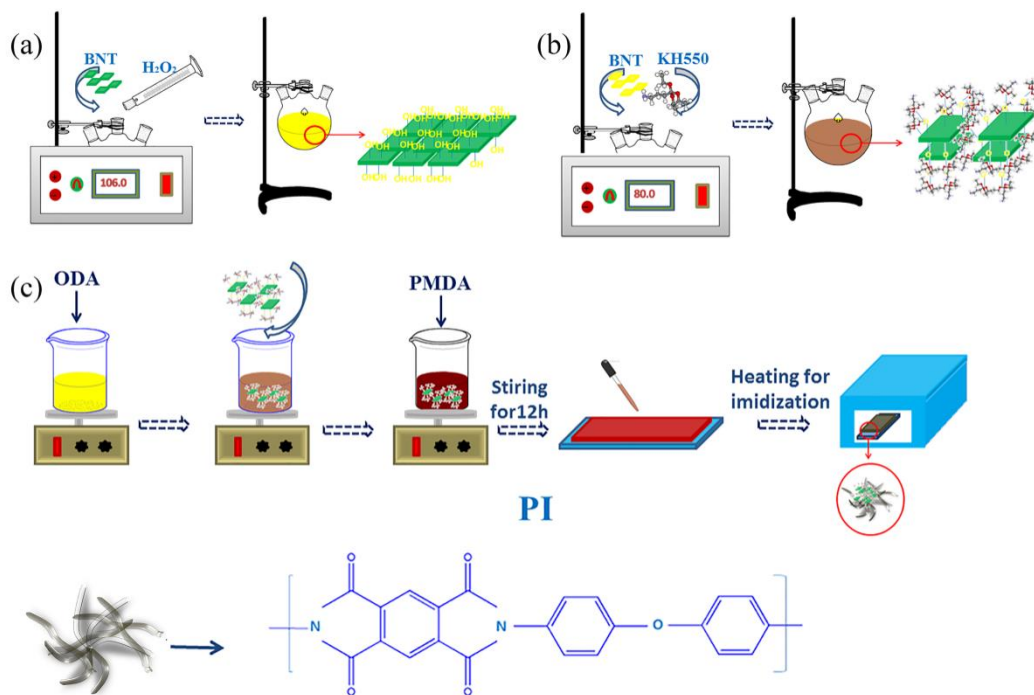


Figure 1. Schematic illustration for preparation processes of BNT/PI composites.

2.5 Characterization

Both sides of composite films were sputtered with 60-nm-thick and 1-mm-diameter gold electrodes for electrical measurements. An E4980A LCR meter (Agilent, Palo Alto, CA, USA) was used to measure dielectric properties of composites from frequency 1 kHz to 1000 kHz at room temperature. The surface and cross-section morphology of the samples was characterized by field emission scanning electron microscope (FESEM, Hitachi, S-4800) equipped with energy dispersive spectroscopy (EDS, OXFORD). Fourier transform infrared spectroscopy (FT-IR) (Bruker IFS66V) was used to characterize the peak position of chemical group of plate-like BNT and pure plate-like BNT. Thermal gravimetric analyzer (TGA; TA, SDT Q600) was used to test the thermal analysis of samples from room temperature to 800 °C of composite film and 1100 °C of the plate-like BNT under an circulation of Ar with a heating rate of 10 °C/min. Phase structure of samples was carried out by a X-ray diffractometer using Cu-K α radiation (XRD, PANalytical X'Pert PRO). The breakdown strength of the BNT/PI was tested by a dielectric withstand voltage test Radiant Technologies, Inc. Albuquerque, NM. *P-E* loops (polarization–electric field loops) were measured by a Premier II ferroelectric test system (Radiant Technologies, Inc. Albuquerque, NM).

3. RESULT AND DISCUSSION

The morphology and microstructure of plate-like BNT were investigated by scanning electron microscopy (SEM) transmission electron microscope (TEM), which are shows in Figure 2 (a), (b) and

(c), as can be seen that the plate-like BNT has a large aspect ratio with a thickness of about 2.5-3.0 μm and a size distribution of between 5 μm \times 5 μm and 15 μm \times 15 μm . The Figure 2 (d) is the diffraction speckles of plate-like BNT from the electron diffraction pattern perpendicular to the plane of the sheet, it can be seen that the orientation of the grains is in the (200) direction. Figure 2 (e) shows the XRD pattern, the diffraction peaks can be readily indexed to a perovskite-structured BNT phase, indicating that the obtained sample is highly crystallized phase of pure BNT [45]. Moreover, EDS analysis is carried out either at residual fine matrix grains or big “brick” grains developed from template grains, as shown in Figure 2 (f). These results suggest that the plate-like BNT templates can diffuse into the matrix and form a single perovskite solid solution [46].

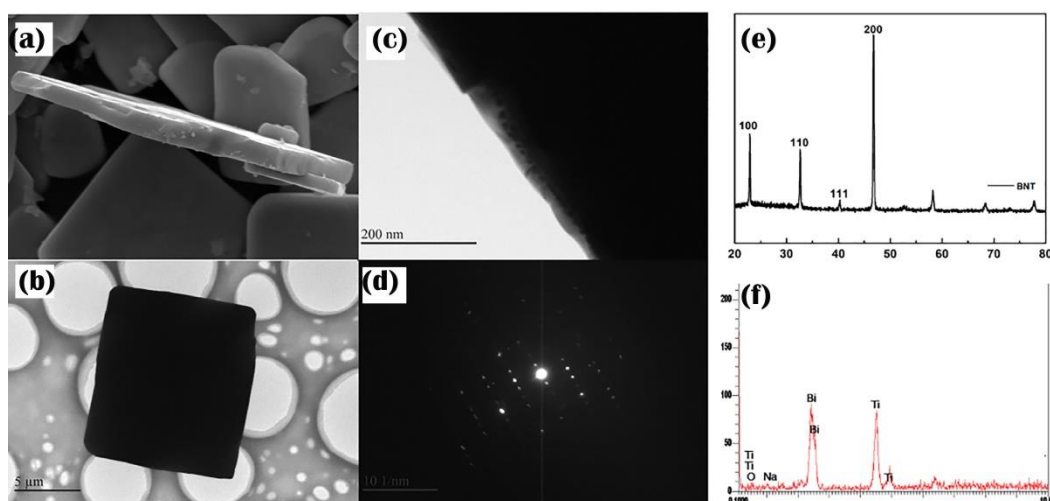


Figure 2. SEM images of (a) and (b) plate-like BNT, (c) high-resolution TEM images of plate-like BNT, (d) the diffraction speckles of plate-like BNT, (e) the XRD patterns of plate-like BNT and (f) the EDS analysis of plate-like BNT.

The FT-IR spectra of pure plate-like BNT and modified plate-like BNT are shown in Figure 3. The peaks near 3100-3700 cm^{-1} are attributed to the stretching vibration peaks of the -OH and -NH groups, which are consistent to the reported results in the literature [47,48]. The -OH stretching vibration peak near 3100 cm^{-1} is weakened after KH550 modification, it indicating that the hydrophilicity of plate-like BNT is weakened during the modification process, while the -NH- stretching vibration peak near 3400 cm^{-1} is significantly enhanced, which indicates that KH550 has been successfully grafted on the surface of plate-like BNT. At the same time, methylene in KH550 has a shoulder at 2800 cm^{-1} and 1100 cm^{-1} , which are the peaks of -C-H and -Si-O-, respectively [49], further demonstrating that the KH550 has been successfully grafted to BNT platelets.

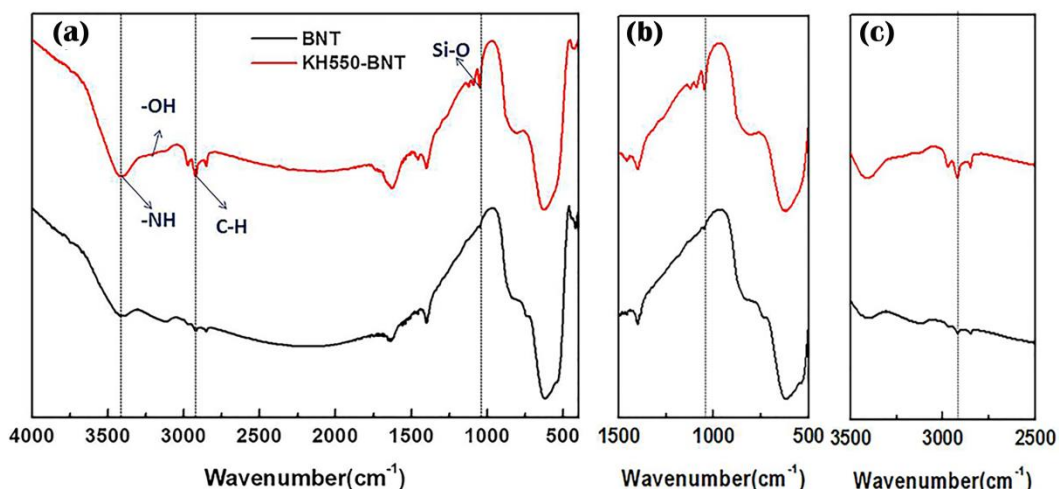


Figure 3. The FT-IR spectra of pure plate-like BNT and KH550 modified plate-like BNT.

The cross-section of the pure PI and the composite film with plate-like BNT (7 wt%) can be seen from Figure 4 (a) and (b), and the light-colored convex sheet-like structure is plate-like BNT, the dark continuous phase is PI matrix, the plate-like BNT is uniformly distributed in the PI matrix, and there is no obvious separation between the BNT and matrix (Figure 4 (b)). These results illustrate that inorganic BNT platelets have good compatibility with PI matrix. It has been well proved that homogeneous dispersion of the filler is a key issue to obtain good dielectric properties [50]. The SEM images of all samples also indicate the high quality and no any apparent pores or voids, and the plate-like BNT can be homogeneously dispersed in PI matrix without large aggregation.

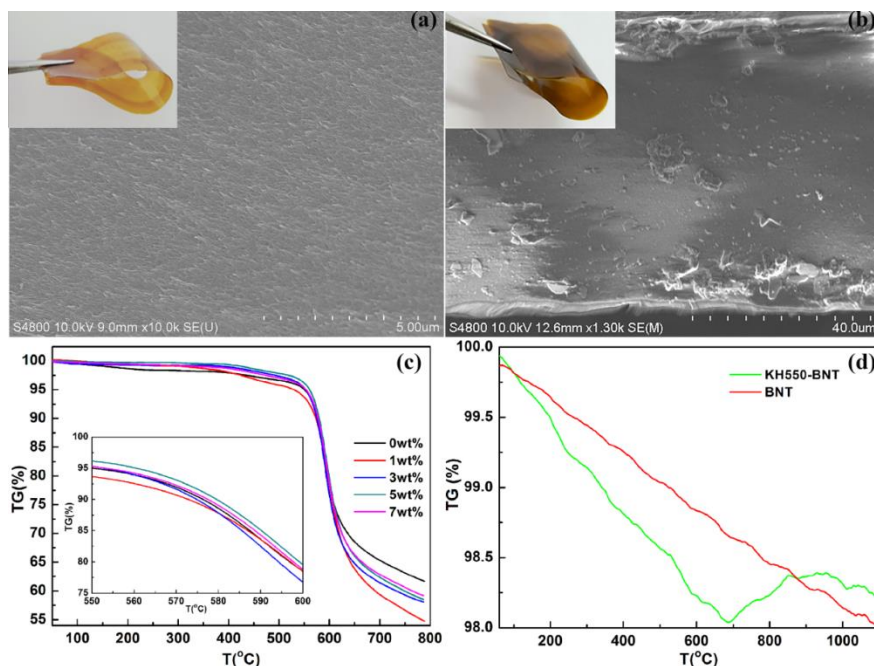


Figure 4. SEM micrographs of the fractured cross section of pure PI (a) and composite films with 5wt% plate-like BNT (b). (c) TGA curves of composite films with different compositions, the inset is the amplified curves between 550-600 °C. (d) TGA curves of plate-like BNT before and after modification.

Figure 5 shows the X-ray diffractograms (XRD) of original and modified BNT samples and composite film with 7 wt% of plate-like BNT. The diffraction peaks can be indexed as rhombohedral perovskite crystal structure of sodium bismuth titanium oxide with the standard pattern of the Joint Committee of Powder Diffraction Standard (JCPDS) code of 36-0340 [51]. The XRD patterns indicate the formation of pure perovskite phase without any secondary phases, which are similar to the previous results [52]. The plate-like BNT has a sharper peak after modification, suggesting that the better crystallinity of the plate-like BNT. By the comparison between the original and modified BNT samples, it is found that only the diffraction peaks of plate-like BNT appear on the XRD patterns after KH550 treatment, and there are no other diffraction peaks, indicating that KH550 has no effect on the crystal structure of plate-like BNT. By comparing pure PI and BNT/PI composite films, both the characteristic peaks of pure PI and BNT could be well distinguished in XRD patterns, which demonstrate that the BNT is well mixed with PI matrix [53], but the peak of BNT/PI composite is more sharper than that of pure PI at $2\theta=22.5^\circ$, suggesting that plate-like BNT has been successfully dispersed in PI matrix .

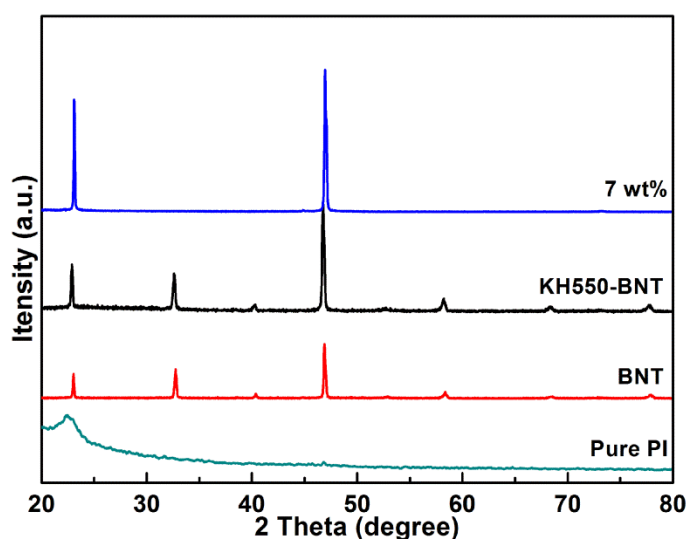


Figure 5. XRD patterns of pure PI, plate-like BNT, KH550 modified plate-like BNT, and composite film of plate-like BNT (7wt%).

Figure 6 shows the variations of the dielectric constant and dielectric loss with frequencies ranging from 1 to 1000 kHz for BNT/PI composites at different mass fractions. The dielectric constant of composites gradually increases with the increasing BNT fillers, which is in agreement with the results of other ceramic/polymer composites [54,55], ranging from 3.47 for pure PI to 14.00 for composites loaded with 5 wt% BNT at 100 kHz, while maintaining a relatively low loss of 0.0061. The dielectric constant increases about 4.03 times compared to that of pure PI. The enhancement of dielectric properties can be well described according to the schematic diagram of Figure 7. When the functionalized plate-like BNT powders are dispersed in the PI matrix (Figure 7), more interfacial regions are formed in combination with anisotropic dielectric behaviors and orientation of plate-like BNT, then leading to a significantly increased dielectric constant, as shown in Figure 7 (c).

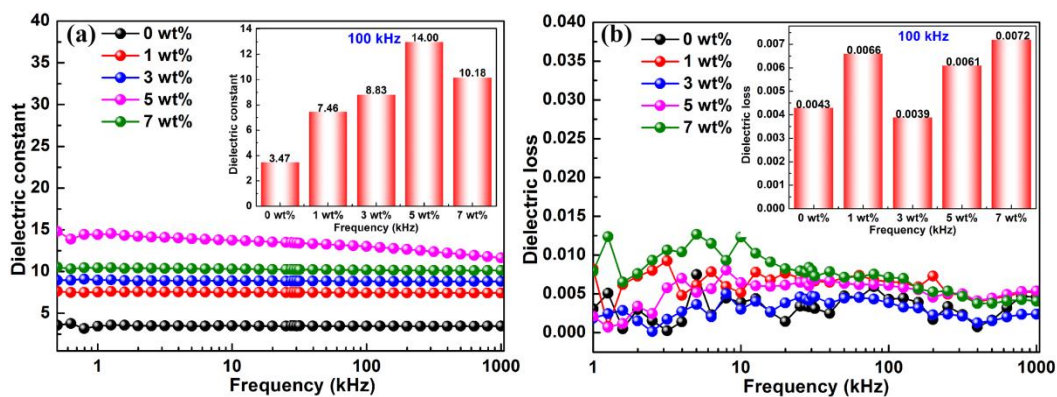


Figure 6. The dependence of the dielectric constant (ϵ_r) (a) and loss ($\text{tg}\delta$) (b) on frequencies for BNT/PI composites (0wt%, 1wt%, 3wt%, 5wt%, and 7wt%). The insets are the dielectric constant and loss values corresponding to the fixed composition and measured frequency (100 kHz).

It is noting that the plate-like BNT can be well aligned in the perpendicular direction to the surface of the composite film after the treatment of tape casting, as shown in Fig. 7 (a), (b) and (c). The dielectric loss remains at a very low value of 0.0061 loaded with 5 wt% of plate-like BNT at 100 kHz. As the frequency increases, the dielectric loss exhibits a continuously decreased trend, as observed in Figure 6 (a). The dielectric constant and loss of BNT/PI composites exhibit a decreased trend with an increase frequency, and all samples with different mass fractions of BNT fillers show a weak dependence on frequency, the phenomenon is clearly related to the interfacial polarization, which does not keep up with the change in frequency at high frequency, leading to the decrease of dielectric constant at high frequency [56].

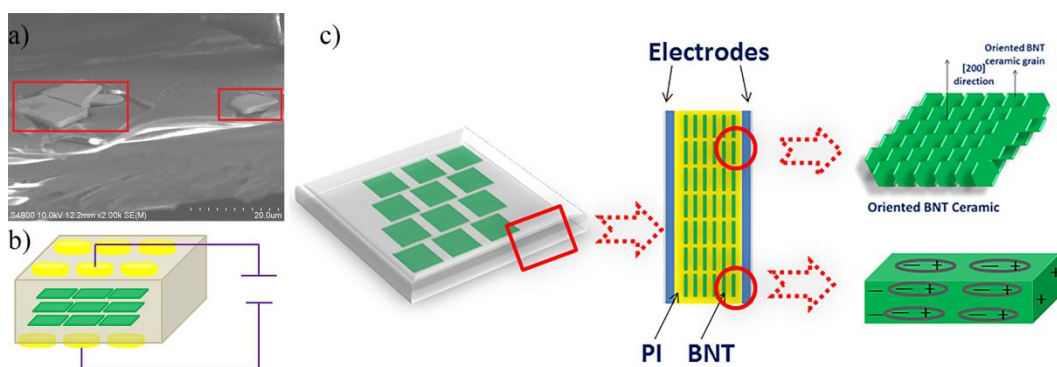


Figure 7 (a) Sectional SEM images of BNT/PI composites, b) the origin of the dielectric behavior of the BNT/PI composites, c) schematic diagram of the formation of numerous dipoles and the orientation of BNT in the BNT/PI composites.

The electric field breakdown strength of composite materials is another important parameter for practical application. The Weibull distribution can be used to analyze the characteristic electrical breakdown strength (BDS), the specific formula is listed as follows:

$$X_i = \ln(E_i) \tag{5}$$

$$Y_i = \ln(-\ln(1 - P_i)) \tag{6}$$

$$P_i = i / (n + 1) \tag{7}$$

Where X_i and Y_i are two factors of the Weibull distribution, E_i is the breakdown strength of BNT/PI composite materials, n is the total number of samples tested in the experiment, P_i is the probability, i is the number of film tests [57]. Breakdown strength can be extracted from the quasi-formula ($Y = 0$) to obtain data points. First, the corresponding breakdown field (E_i) and all other dates are calculated and listed in numerical order ($E_1 \leq E_2 \leq E_3 \dots \leq E_i \leq \dots \leq E_n$). As shown in Figure 8, the two-parameter Weibull distribution can be used to analyze the breakdown strength characteristics [58]:

$$P(E) = 1 - \left(-\left(\frac{E}{E_B}\right)\beta\right) \tag{8}$$

Where $P(E)$ is the cumulative probability of electric failure, E is breakdown strength, E_B is the characteristic breakdown strength, and β is associated with the linear regressive fit of the distribution [59]. To guarantee the reliability of breakdown strength, four samples are provided for every composite film. It can be seen that the breakdown strength of the composites is decreased with the increase of plate-like BNT contents. All of the composites show excellent insulating property, the value of the breakdown strength reaches 1267kV/cm even when the content of the plate-like BNT is up to 7wt%.

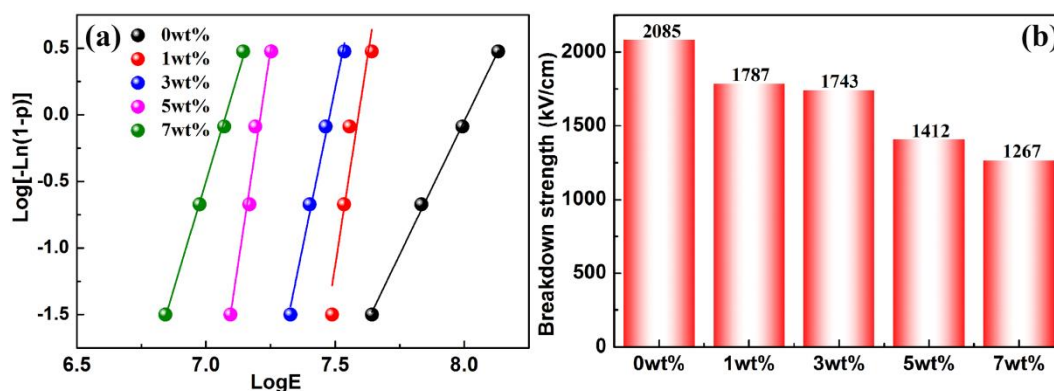


Figure 8. a) Weibull distribution of the dielectric breakdown strength of composite materials, b) the average breakdown strength of composites filled with different plate-like BNT contents.

The effects of the polarization of polymer matrix on the dielectric behavior are better revealed by P-E loops of PI-based composites (Figure 9). The polarization intensity is further increased upon the introduction of plate-like BNT. As shown in Figure 9, at the same electric field of 700 kV/cm, the maximal polarization increases monotonically from 0.559 $\mu\text{C cm}^{-2}$ to 1.016 $\mu\text{C cm}^{-2}$ as the content of plate-like BNT ceramics increases from 0wt% to 7wt%. Meanwhile, the remanent polarization (P_r) remains at a very low value, almost near to zero. According to the P-E loops, the BNT/PI composite films almost show a linear dielectric performance, so we can calculate its energy storage density by the equation (1). The calculated results are shown in Table 2, the energy storage density reaches its maximum of 1.27 J/cm^3 at a filler content of 5 wt%, which is about twice as large as that of the pure PI. The composite materials with high dielectric properties (high dielectric constant and low dielectric loss) is urgently required. The dielectric properties of PI-based composites are listed in Table 2. The results show that the BNT/PI composites have a great advantage in comparison with other composite materials,

possessing both a high dielectric constant and a very low dielectric loss, and have excellent flexibility due to its low filling content. So, the composites are found to be potentially useful in embedded capacitors.

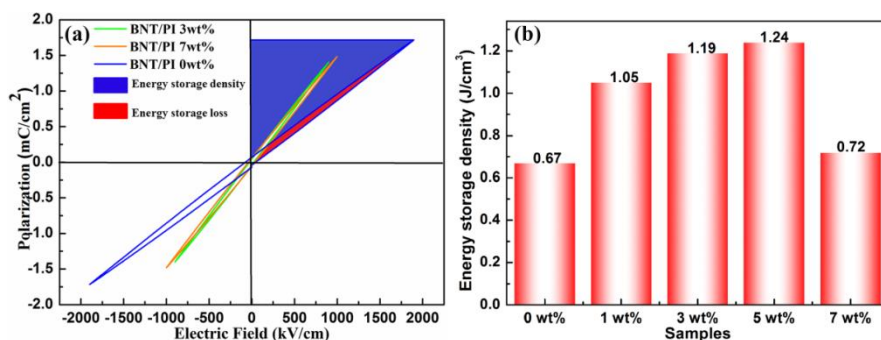


Figure 9. a) Room temperature P - E loops of BNT/PI composites (0wt%, 3wt%, 7wt%), b) energy storage density of PI-based composites filled with different volume fraction of plate-like BNT.

Table 1. Dielectric properties of PI-based composites.

PI-based composites	Dielectric constant	Dielectric loss	Breakdown strength (kV/mm)	Reference
BaTiO ₃ /PI (3 vol%)	27	0.015	--	[15]
BaTiO ₃ /PI (50 vol%)	28.93	0.0084	--	[16]
BaTiO ₃ /PI (9 vol%)	6.8	0.012	--	[17]
mBN/PI (26 vol%)	3.77	0.007	--	[20]
SiO ₂ /PI (20 wt%)	79	0.25	--	[35]
Ba _{0.7} Sr _{0.3} TiO ₃ /PI (10 vol%)	6.2	<0.04	--	[36]
BaTiO ₃ /PI (50 vol%)	19.03	0.0109	--	[37]
BaTiO ₃ /PI (50 vol%)	14.64	0.01	--	[38]
BaTiO ₃ /PI (10 vol%)	7.3	0.11	--	[39]
Bi _{0.5} Na _{0.5} TiO ₃ /PI (5 wt%)	14.00	0.0061	126.7	This work

Table 2. Dielectric and energy storage properties of BNT/PI composite films.

Samples	Dielectric constant (100 kHz)	Dielectric loss (100 kHz)	Breakdown strength (kV/cm)	Energy storage density (J/cm ³)	Thickness of samples (mm)
0wt%	3.47	0.0043	2085	0.67	0.020
1wt%	7.46	0.0066	1787	1.05	0.038
3wt%	8.83	0.0039	1743	1.19	0.042
5wt%	14.00	0.0061	1412	1.24	0.050
7wt%	10.18	0.0072	1267	0.72	0.043

4. CONCLUSIONS

In this paper, the plate-like BNT/PI composites have been prepared by in-situ polymerization method. And the plate-like $\text{Na}_{0.5}\text{Bi}_{0.5}\text{TiO}_3$ (BNT) was fabricated by two-step molten salt method. The results showed that the plate-like BNT fillers lead to a significant increase of dielectric constant ($\epsilon_r=14.00$) at a very low content, which is 4.03 times as large as that of pure PI ($\epsilon_r=3.47$) when BNT content is about 5 wt%, while maintaining a relatively low loss ($\text{tg}\delta=0.0061$) and high breakdown strength (1412 kV/cm). The measured energy density for the sample with 5 wt% BNT content increased to a value of 1.24 J/cm^3 , higher than that of pure PI (0.67 J/cm^3). These results suggest that the plate-like BNT/PI composites could have potential applications in energy storage devices.

ACKNOWLEDGEMENT

This work was supported by the Natural Science Foundation of China (No. 51462028), the Natural Science Foundation of Inner Mongolia (No. 2016MS0208), Program for Young Talents of Science and Technology in Universities of Inner Mongolia Autonomous Region (NJYT-17-A10).

References

1. Z. Pan, B. Liu, J. Zhai, L. Yao, K. Yang, *Nano. Energy*, 40 (2017) 587-595.
2. Q. Chen, Y. Shen, S. Zhang, Q. M. Zhang, *Annu. Rev. Mater. Res.*, 45 (2015) 433-458.
3. X. Chen, X. Han, Q. Shen, *Adv. Electron. Mater.*, 3 (2017) 1600460.
4. Z. Dang, J. Yuan, S. Yao, R. Liao, *Adv. Mater.*, 25 (2013) 6334-6365.
5. L. Zhang, Z. Liu, X. Lu, G. Yang, X. Zhang, Z. Cheng, *Nano. Energy*, 26 (2016) 550-557.
6. P. Prateek, V. Thakur, R. Gupta, *Chem. Rev.*, 116 (2016) 4260-4317.
7. T. Huan, S. Boggs, G. Teysse, C. Laurent, M. Cakmak, S. Kumar, *Prog. Mater. Sci.*, 83 (2016) 236-269.
8. J. Biggs, K. Danielmeier, J. Hitzbleck, J. Krause, T. Kridl, *Angew. Chem., Int. Ed.*, 52 (2013) 9409-9421.
9. Z. Dang, J. Yuan, S. Yao, R. Liao, *Adv. Mater.*, 25 (2013) 6334-6365.
10. Y. Cao, P. Irwin, K. Younsi, *IEEE Trans. Dielectr. Electr. Insul.*, 11 (2004) 797-807.
11. B. Chu, X. Zhou, K. Ren, B. Neese, M. Lin, Q. Wang, *Science*, 313 (2006) 334-336.
12. M. F. Lin, V. K. Thakur, E. J. Tan, P. S. Lee, *RSC Adv.*, 1 (2011) 827-836.
13. E. Q. Huang, J. Zhao, J. W. Zha, L. Zhang, R. J. Liao and Z. M. Dang, *J. Mater. Chem.*, 115 (2014) 797.
14. S. Luo, Y. Shen, S. Yu, Y. Wan, W. Liao, *Energy & Environmental Science*, 10 (2016) 137-144.
15. Y. H. Wu, J. W. Zha, Z. Q. Yao, F. Sun, R. K. Li, Z. M. Dang, *RSC Advances*, 5 (56) (2015) 44749-44755.
16. Y. Ding, Q. Wu, D. Zhao, W. Ye, M. Hanif, *European Polymer Journal*, 49 (2013) 2567-2571.
17. M. Wang, W. L. Li, Y. Feng, Y. F. Hou, T. D. Zhang, W. D. Fei, J. H. Yin, *Ceramics International*, 41(10) (2015) 13582-13588.
18. S. Su, R. Zuo, D. Lv, J. Fu, *Powder Technology*, 217 (2012) 11-15.
19. P. Li, J. Zhai, B. Shen, S. Zhang, X. Li, *Advanced Materials*, 30 (2018) 1705171.
20. Y. Deng, Y. Zhang, Y. Wang, M. Li, J. Yuan, *Composites, Part A.*, 43 (2012) 842-846.

21. J. Gu, Z. Lv, Y. Wu, Y. Guo, L. Tian, *Composites Part A Applied Science & Manufacturer*, 94 (2017) 209-216.
22. J. Waanders, Eindhoven: Philips Components, 1991.
23. X. Kong, Y. Ishikawa, K. Shinagawa, Q. Feng, *J. Am. Ceram. Soc.*, 94 (2011) 3716-3721.
24. L. Wang, F. Gao, J. Xu, K. Zhang, J. Kong, *Composites Science & Technology*, 158 (2018) 112-120.
25. H. Luo, Z. Wu, X. Zhou, Z. Yan, K. Zhou, *Composites Science & Technology*, 160 (2018) 237-244.
26. Y. Bin, K. Oishi, A. Koganemaru, D. Zhu, M. Matsuo, *Carbon*, 43 (2005) 1617-1627.
27. H. Y. Lu, C. Y. Chou, J. H. Wu, J. J. Lin, G. S. Liou, *J. Mater. Chem. C.*, 3 (2015) 3629-3635.
28. X. F. Lei, Y. Chen, H. P. Zhang, X. J. Li, P. Yao, *ACS Appl. Mater. Inter.*, 5 (2013) 10207-10220.
29. X. Liu, J. Yin, Y. Kong, M. Chen, Y. Feng, Z. Wu, *Thin Solid Films*, 544 (2013) 54-58.
30. A. Alias, Z. Ahmad A. Ismail, *Mater. Sci. Eng. B.*, 176 (2011) 799-804.
31. K. Abe, D. Nagao, A. Watanabe, M. Konno, *Polym. Int.*, 62 (2013) 141-145.
32. C. Hamciuc, E. Hamciuc, M. Olariu, R. Ciobanu, *Polym. Int.*, 59 (2010) 668-675.
33. E. Hamciuc, C. Hamciuc, I. Bacosca, M. Cristea, L. Okrasa, *Polym. Compos.*, 32 (2011) 846-855.
34. Q. Chi, J. Sun, C. Zhang, G. Liu, J. Lin, Y. Wang, X. Wang, Q. Lei, *J. Mater. Chem. C.*, 2 (2014) 172-177.
35. Z. M. Dang, T. Zhou, S. H. Yao, J. K. Yuan, J. W. Zha, *Adv. Mater.*, 21 (2009) 2077-2082.
36. L. Liu, F. Lv, Y. Zhang, P. Li, W. Tong, L. Ding, *Compos. A App. Sci. Manu.*, 99 (2017) 41-47.
37. C. Beier, J. Sanders, R. Brutchey, *J. Phys. Chem. C.*, 117 (2013) 6958-6965.
38. W. Sun, X. Lu, J. Jiang, X. Zhang, P. Hu, M. Li, Y. Shen, *Journal of Applied Physics*, 121(24) (2017) 244101.
39. S. H. Choi, I. D. Kim, J. M. Hong, K. H. Park, S. G. Oh, *Materials Letters*, 61(11-12) (2007) 2478-2481.
40. X. Fang, X. Liu, Z. Cui, J. Qian, J. Pan, *Journal of Materials Chemistry A.*, 3 (2015) 10005-10012.
41. Z. M. Dang, H. Y. Wang, H. P. Xu, *Applied physics letters*, 89 (2006) 112902.
42. Z. M. Dang, Y. F. Yu, H. P. Xu, J. Bai, *Composites Science and Technology*, 68 (2008) 171-177.
43. H. P. Xu, Z. M. Dang, M. J. Jiang, S. H. Yao, J. Bai, *Journal of Materials Chemistry*, 18 (2008) 229-234.
44. W. Xia, Z. Xu, F. Wen, Z. Zhang, *Ceramics International*, 38 (2012) 1071-1075.
45. D. Lv, R. Zuo, *Journal of Alloys and Compounds*, 560 (2013) 62-66.
46. S. Su, R. Zuo, *Journal of Alloys and Compounds*, 525 (2012) 133-136.
47. B. Wei, Q. Chang, C. Bao, L. Dai, G. Zhang, F. Wu, *Colloids and Surfaces A: Physicochemical and Engineering Aspects*, 434 (2013) 276-280.
48. L. Fan, C. W. Nan, S. Zhao, *Solid State Ionics*, 164 (1-2) (2003) 81-86.
49. M. J. Jiang, Z. M. Dang, S. H. Yao, J. Bai, *Chemical physics letters*, 457 (4-6) (2008) 352-356.
50. Z. M. Dang, J. K. Yuan, S. H. Yao, R. J. Liao, *Advanced Materials*, 25 (44) 6334-6365.
51. C. L. Guo, Y. Q. Wu, T. B. Wang, Wuli Xuebao: *Acta Phys. Sin.* 31 (1982) 1119.
52. T. Motohashi, T. Kimura, *Journal of the European Ceramic Society*, 27(13-15) (2007) 3633-3636.
53. W. Sun, X. Lu, J. Jiang, X. Zhang, P. Hu, M. Li, Y. Shen, *Journal of Applied Physics*, 121 (24) (2017) 244101.
54. Z. M. Dang, T. Zhou, S. H. Yao, J. K. Yuan, J. W. Zha, H. T. Song, *Adv. Mater.*, 21 (20) (2009) 2077-2082.
55. Z. F. Zhang, X. F. Bai, J. W. Zha, W. K. Li, Z. M. Dang, *Compos. Sci. Technol.*, 97 (2014) 100-105.
56. M. Tian, Q. Ma, X. L. Li, L. Q. Zhang, T. Nishic, N. Y. Ning, *J. Mater. Chem. A* 2 (29) (2014) 11144-11154.
57. T. Zhou, J. W. Zha, Y. Hou, D. R. Wang, J. Zhao and Z. M. Dang, *ACS Appl. Mater. Interfaces*, 2011, 3, 4557-4560.
58. Y. Hernandez, V. Nicolosi, M. Lotya, F. M. Blighe, Z. Y. Sun, S. De, I. T. McGovern, B. Holland, M. Byrne, Y. K. Gun'Ko, J. J. Boland, P. Niraj, G. Duesberg, S. Krishnamurthy, R. Goodhue, J.

Hutchison, V. Scardaci, A. C. Ferrari and J. N. Coleman, *Nature Nanotechnology*, 3 (2008) 563-568.

59. X. Zheng, H. Yu, S. Yue, R. Xing, Q. Zhang, Y. Liu, B. Zhang, *Int. J. Electrochem. Sci.*, 13 (2018) 1-13.

© 2019 The Authors. Published by ESG (www.electrochemsci.org). This article is an open access article distributed under the terms and conditions of the Creative Commons Attribution license (<http://creativecommons.org/licenses/by/4.0/>).